Crystal Structure of Glycosomal Glyceraldehyde-3-phosphate Dehydrogenase from *Leishmania mexicana*: Implications for Structure-Based Drug Design and a New Position for the Inorganic Phosphate Binding Site[†,‡]

Hidong Kim,[§,||] Ingeborg K. Feil,[§,||] Christophe L. M. J. Verlinde,[||] Philip H. Petra,[⊥] and Wim G. J. Hol*[,§,||,⊥]

Howard Hughes Medical Institute and Departments of Biological Structure and Biochemistry, University of Washington, Box 357742, Seattle, Washington 98195

Received July 20, 1995; Revised Manuscript Received September 11, 1995[⊗]

ABSTRACT: The structure of glycosomal glyceraldehyde-3-phosphate dehydrogenase (GAPDH) from the trypanosomatid parasite *Leishmania mexicana* has been determined by X-ray crystallography. The protein crystallizes in space group $P2_12_12_1$ with unit cell parameters $a = 99.0$ Å, $b = 126.5$ Å, and $c = 138.9$ Å. There is one 156 000 Da protein tetramer per asymmetric unit. The model of the protein with bound NAD^+s and phosphates has been refined against 86% complete data from 10.0 to 2.8 Å to a crystallographic R_{factor} of 0.198. Density modification by noncrystallographic symmetry averaging was used during model building. The final model of the *L. mexicana* GAPDH tetramer shows small deviations of less than 0.5° from ideal 222 molecular symmetry. The structure of *L. mexicana* GAPDH is very similar to that of glycosomal GAPDH from the related trypanosomatid *Trypanosoma brucei*. A significant structural difference between *L. mexicana* GAPDH and most previously determined GAPDH structures occurs in a loop region located at the active site. This unusual loop conformation in *L. mexicana* GAPDH occludes the inorganic phosphate binding site which has been seen in previous GAPDH structures. A new inorganic phosphate position is observed in the *L. mexicana* GAPDH structure. Model building studies indicate that this new anion binding site is well situated for nucleophilic attack of the inorganic phosphate on the thioester intermediate in the GAPDH-catalyzed reaction. Since crystals of *L. mexicana* GAPDH can be grown reproducibly and diffract much better than those of *T. brucei* GAPDH, *L. mexicana* GAPDH will be used as a basis for structure-based drug design targeted against trypanosomatid GAPDHs.

Species of the family Trypanosomatidae are protozoan parasites which cause a wide variety of severely destructive diseases. Some of the most serious of these diseases are African sleeping sickness, the causative agents of which are subspecies of *Trypanosoma brucei*, and Chagas' disease, the causative agent of which is *Trypanosoma cruzi*. Sleeping sickness is one of the world's major tropical diseases as 50 million people in Africa are at risk of developing this disease (Kuzoe, 1993). If untreated, the disease is virtually always fatal. Current drug therapies are plagued by such problems as resistance and toxicity to the patient (Bellofatto *et al.*, 1987; Veeken *et al.*, 1989; Kuzoe, 1993; Wang, 1995). In the New World, Chagas' disease is one of the leading causes of heart failure in Central and South America (Tanowitz *et al.*, 1992). There are currently no satisfactory drugs for the treatment of Chagas' disease (Kirchhoff, 1993). The closely related trypanosomatids of genus *Leishmania* are also the causative agents of a variety of diseases collectively known as leishmaniases. One of the most common species of *Leishmania* is *L. mexicana*, which is distributed throughout Central and South America and the southern United States. *L. mexicana* infection can lead to diffuse cutaneous leishmaniasis, a disease similar to lepromatous leprosy (Maingon *et al.*, 1994). Drugs used to treat leishmaniases are also hampered by the same problems associated with sleeping sickness drugs, such as side effects and resistance (Grogl *et al.*, 1991). Considering that there are over 30 million people worldwide infected with species of *Trypanosoma* and *Leishmania* (Kolberg, 1994), there is a great need for new, more effective drugs to treat the diseases caused by these organisms.

In the search for more effective trypanocidal drugs, there are certain peculiarities in the biology of trypanosomatids which appear to be exploitable. Trypanosomatids are highly dependent on glycolysis as a source of ATP production. In fact, the host bloodstream form of *T. brucei* is entirely dependent on glycolysis for ATP production as it has no functional tricarboxylic acid cycle (Opperdoes, 1987). Indeed, compounds which inhibit glycolysis have been shown to be trypanocidal (Opperdoes & Borst, 1977; Fairlamb *et al.*, 1977; Clarkson & Brohn, 1976). Trypanosomatids possess a specialized microbody organelle, the glycosome, which sequesters the first seven enzymes of the glycolytic pathway. In trypanosomatids, the glycolytic flux from glucose to 3-phosphoglycerate occurs entirely within the glycosome (Opperdoes & Borst, 1977), and no parallel pathway exists in the cytosol (Visser *et al.*, 1981). This great dependence on glycolysis as a source of energy supply in trypanosomatids makes the glycolytic enzymes attractive targets for trypanocidal drug design. We are currently working on structure-based drug design (Verlinde & Hol,

[†] This research was supported in part by a major equipment grant from the Murdock Charitable Trust.

[‡] The coordinates of the LmGAPDH structure have been deposited in the Brookhaven Protein Data Bank under access code 1GYP.

* To whom correspondence should be addressed.

[§] Howard Hughes Medical Institute.

[||] Department of Biological Structure.

[⊥] Department of Biochemistry.

[⊗] Abstract published in *Advance ACS Abstracts,* November 1, 1995.

0006-2960/95/0434-14975$09.00/0

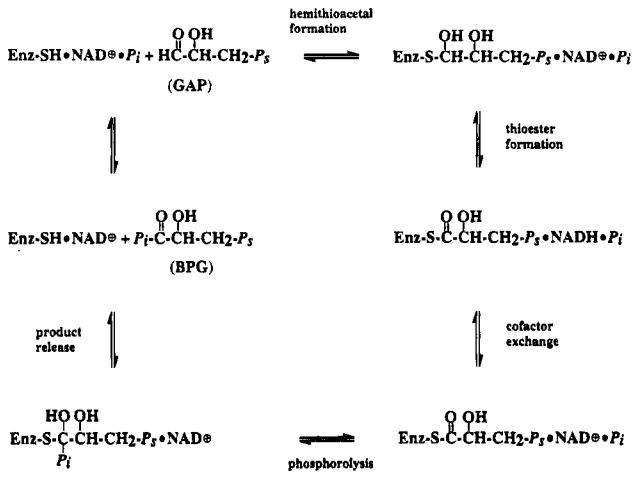

FIGURE 1: Reaction mechanism of GAPDH (Segal & Boyer, 1953; Harrigan & Trentham, 1973; Harris & Waters, 1976). SH denotes the essential Cys. GAP is glyceraldehyde 3-phosphate, and BPG is 1,3-bis(phosphoglycerate). The substrate phosphate and inorganic phosphate are denoted by P_s and P_i, respectively. Covalent bonds are represented by lines, and noncovalent interactions are represented by dots.

1994; Verlinde *et al.*, 1994a) directed against the trypanosomatid glycolytic enzymes. As part of our continuing efforts, we report here the three-dimensional structure determination of glycosomal glyceraldehyde-3-phosphate dehydrogenase (GAPDH)[1] from *L. mexicana* by X-ray crystallography.

L. mexicana GAPDH (LmGAPDH) is a homotetrameric enzyme of total molecular mass 156 000 Da.[2] It catalyzes the oxidative phosphorylation of glyceraldehyde 3-phosphate (GAP) to 1,3-bis(phosphoglycerate) (BPG). NAD^+ is an essential cofactor in the reaction. The accepted mechanism of the GAPDH-catalyzed reaction involves an initial formation of a covalent hemithioacetal intermediate between GAP and an essential Cys (Cys-166 in LmGAPDH). The hemithioacetal is then oxidized to a thioester, with concomitant reduction of NAD^+ to NADH. The product BPG is finally released by phosphorolytic attack on the thioester by an inorganic phosphate (Figure 1). NAD^+ is not only required for the oxidation of the hemithioacetal to the thioester but also enhances the phosphorolysis of the thioester (Racker & Krimsky, 1958). In addition to the essential Cys, there is also an active site His (His-194 in LmGAPDH) which is conserved in all known GAPDHs. This His appears to activate the essential Cys and also to facilitate formation of tetrahedral intermediates (Polgár, 1975; Soukri *et al.*, 1989).

Although the three-dimensional structure of *T. brucei* GAPDH (TbGAPDH) had been determined (Vellieux *et al.*, 1993, 1995), difficulties in obtaining ample amounts of protein and in crystallization rendered this isozyme not extremely well suited for structure-based drug design. For these reasons, we have turned our attention to LmGAPDH. The 81% sequence identity between LmGAPDH and TbGAPDH (Hannaert *et al.*, 1992) results in similar structures for these two isozymes, most notably at the cofactor binding site, which is presently being studied as a possible drug binding target (Verlinde *et al.*, 1994b). Since LmGAPDH is more readily purified and crystallized than TbGAPDH is, crystallographic studies on LmGAPDH−ligand complexes will likely allow us to further develop the selective inhibitors of GAPDH which have already been designed by molecular modeling (Verlinde *et al.*, 1994b).

A particularly noteworthy aspect of the LmGAPDH structure determination is the crystallization environment of LmGAPDH. Previous structures of GAPDHs have been determined from crystals grown in high $(NH_4)_2SO_4$ concentrations, and bound sulfates were taken to indicate the positions of the phosphate binding sites in these GAPDHs. LmGAPDH crystals, in contrast, were grown from a rather unusual low-salt medium which contained phosphate instead of sulfate. The 200 mM phosphate concentration of the LmGAPDH crystallization medium is closer to physiological phosphate concentrations than are the much higher, ~2 M, sulfate concentrations from which previous GAPDH crystals were grown. Associated with this more physiological crystallization medium, the structure of LmGAPDH reported here shows an unusual loop conformation at the active site and a repositioning of the inorganic phosphate binding site, compared with previous structures of GAPDHs. The implications of this structure on drug design, as well as on GAPDH catalysis in general, will be discussed.

MATERIALS AND METHODS

Preparation and Purification of L. mexicana GAPDH. LmGAPDH was prepared and purified according to a modification of a previously reported procedure (Hannaert *et al.*, 1994). LmGAPDH-overproducing *Escherichia coli* were grown and lysed as previously described (Hannaert *et al.*, 1994). The cell lysate was centrifuged at 16000*g* for 30 min. The supernatant was passed through a $1^1/_4$ in. 27-gauge needle to reduce the viscosity of the sample and then purified by hydrophobicity chromatography in which LmGAPDH was eluted with a decreasing $[(NH_4)_2SO_4]$ gradient (Hannaert *et al.*, 1994). Eluted fractions containing LmGAPDH were pooled and dialyzed against $(NH_4)_2SO_4$-free buffer. The dialyzed sample was then purified by cation-exchange chromatography in which LmGAPDH was eluted with an increasing [KCl] gradient (Hannaert *et al.*, 1994). The LmGAPDH sample from the cation-exchange column was further purified over a 2.5 cm (diameter) × 120 cm (length) Sephacryl S-200 gel filtration column. The elution buffer was 0.1 M triethanolamine/1 mM NAD^+/200 mM KCl/1 mM DTT/1 mM EDTA/1 mM PMSF/1 μM leupeptin/1 μM pepstatin A, pH 7.6, and the flow rate was 14 mL/h. Fractions containing LmGAPDH as judged by activity assays and SDS−PAGE were pooled and concentrated to 10 mg/mL in the elution buffer.

Crystallization and X-Ray Diffraction Data Collection. Crystals of LmGAPDH were grown by sitting drop vapor diffusion against a reservoir buffer of 0.2 M sodium phosphate/27.5% PEG-1000, pH 7.0 (pH adjusted with 0.2 M citric acid). The sitting drops were initially set up with equal volumes of 10 mg/mL LmGAPDH solution and

[1] Abbreviations: GAPDH, glyceraldehyde-3-phosphate dehydrogenase; LmGAPDH, *Leishmania mexicana* glycosomal GAPDH; TbGAPDH, *Trypanosoma brucei* glycosomal GAPDH; BsGAPDH, *Bacillus stearothermophilus* GAPDH; TmGAPDH, *Thermotoga maritima* GAPDH; MBDA, 2′-deoxy-2′-(*m*-methoxybenzamido)adenosine; GAP, glyceraldehyde 3-phosphate; BPG, 1,3-bis(phosphoglycerate); rms, root mean square; F_o and F_c, observed and calculated structure factors.

[2] There are actually two GAPDH isozymes in species of *Trypanosoma* and *Leishmania*, one contained in the glycosome and the other in the cytosol (Hannaert *et al.*, 1992). The function of the cytosolic GAPDH is unclear as there is no glycolysis or gluconeogenesis in the cytosol (Visser *et al.*, 1981). All further references to trypanosomatid GAPDH herein will be to the glycosomal isozyme.

reservoir buffer. Crystals grew within 2 weeks as rectangular bars with dimensions of 0.3 mm × 0.3 mm × 1.0 mm. Precession photographs identified the space group as $P2_12_12_1$ with unit cell parameters $a = 99.0$ Å, $b = 126.5$ Å, and $c = 138.9$ Å. The cell volume was consistent with one 156 000 Da LmGAPDH tetramer per asymmetric unit.

Since knowledge of anion binding is critical in any discussion of the GAPDH-catalyzed reaction, it is important to note the anion environment of the LmGAPDH purification and crystallization. Due to the protocol used in the purification and crystallization of LmGAPDH, the bound anions seen in the present LmGAPDH structure are almost certainly phosphates and not sulfates, as have been seen in previous GAPDH structures. The cell lysis buffer in the preparation of LmGAPDH contained $(NH_4)_2SO_4$, and the first of the three columns employed in the purification (the hydrophobicity column) involved elution buffers containing $(NH_4)_2SO_4$ (Hannaert *et al.*, 1994). Thereafter, however, the LmGAPDH sample was dialyzed against $(NH_4)_2SO_4$-free buffer, and the buffers used in the two subsequent columns (cation exchange and gel filtration), the protein storage buffer, and the crystallization buffer contained no $(NH_4)_2SO_4$. Any sulfate in the crystallization of LmGAPDH could have been introduced only as trace impurities in the reagent grade chemicals which were used.

Monochromatic X-ray diffraction data were collected at the Stanford Synchrotron Radiation Laboratory. The wavelength of the incident radiation was 1.08 Å, and diffraction spots were recorded on the MAR area detector. All of the data used in the LmGAPDH structure determination were recorded from a single crystal cooled to 5 °C with an air stream. The data were processed using MOSFLM. A total of 137 752 reflections between 30.0 and 2.8 Å resolution were reduced to 37 522 unique reflections (86% completeness). Overall, the data set has an R_{sym} of 0.076 on intensities [$R_{sym} = \sum_{hkl}(\sum_i|I - \bar{I}|/\sum_i I)$]. The last resolution shell of data, containing reflections from 2.87 to 2.80 Å resolution, is 77% complete and has an R_{sym} of 0.128 on intensities.

Structure Determination and Preliminary Refinement. The structure of LmGAPDH was determined by molecular replacement. The structure of the crystal form II TbGAPDH tetramer minus the bound NAD^+s and sulfates (Vellieux *et al.*, 1993; R. J. Read, 1993, unpublished results) was used as the search model. The overall sequence identity between LmGAPDH and TbGAPDH is 81% (Hannaert *et al.*, 1992). The differences in sequence between these two GAPDHs include an N-terminal Ala insertion in LmGAPDH. The program ALMN in the CCP4 suit of programs was used for the rotation function. Model structure factors were calculated from the search model placed in an orthogonal $P1$ cell with dimensions of 110 Å × 110 Å × 110 Å. The rotation search using data from 7.0 to 5.0 Å within a Patterson integration radius of 30 Å resulted in four equally prominent peaks which were related by noncrystallographic 222 symmetry as was expected for one tetramer per asymmetric unit in the LmGAPDH crystal. These were the highest peaks in the rotation function, with peak heights 6σ above the mean. The search model was rotated by the rotation solution $\alpha = 101.5°$, $\beta = 89.3°$, and $\gamma = 125.1°$ (Crowther convention). A translation search was executed with X-PLOR using the rotated search model and data from 8.0 to 5.0 Å. There was a single prominent peak 21σ above the mean for the translation search corresponding to $X = 39.6$ Å, $Y = 28.5$ Å, and $Z = 50.3$ Å.

The rotated and translated search model was then rigid-body refined, with only the quaternary structure of the search model tetramer being allowed to change while the four individual subunits were held as rigid bodies. During this refinement, the R_{factor} ($R_{factor} = \sum_{hkl}||F_o| - |F_c||/|F_o|$) decreased from 0.413 to 0.349 with respect to data from 8.0 to 4.0 Å. At this point, the residues in the TbGAPDH model which are not conserved in LmGAPDH were changed to alanine, except for nonconserved residues which are glycine in LmGAPDH, which were changed to glycine in the model. This "multi-alanine" model was refined by Powell minimization with noncrystallographic symmetry restraints against data from 8.0 to 3.0 Å. The R_{factor} dropped from 0.370 to 0.302. A $2F_o - F_c$ electron density map calculated from this model showed density in the cofactor binding sites which was clearly interpretable as NAD^+. One cofactor was built into the appropriate density in each of the four subunits.

Density Modification and Final Refinement. Iterative density modification by noncrystallographic symmetry averaging was executed with the DEMON suite of programs (Vellieux & Read, 1995). The initial molecular envelope was generated from the multi-alanine LmGAPDH tetramer with NAD^+s. The maps used for density modification were Sim weighted (Sim, 1959) $2F_o - F_c$ maps. Density modification was begun with a map calculated with data from 30.0 to 4.0 Å. The resolution was gradually extended in steps of 0.02 Å with one round of density modification at each new resolution. At 3.20 Å, 55 of the 71 nonconserved residues between LmGAPDH and TbGAPDH spanning Pro-2 through Ser-358 in LmGAPDH were replaced with the correct LmGAPDH residues according to the averaged Sim weighted $2F_o - F_c$ map.

The model used up to this point had slight deviations from ideal 222 molecular symmetry. The deviations from ideal 2-fold symmetry in the three molecular axes were less than 0.5°. Model refinements of an ideal 222 tetramer indicated this deviation from ideal point group symmetry to be a real structural feature of the LmGAPDH tetramer and not merely a computational artifact. Rigid-body refinements starting from an ideal 222 tetramer, during which the individual subunits were allowed to move with respect to each other, against data from 10.0 to 4.0 Å, 10.0 to 3.2 Å, and 10.0 to 2.8 Å converged to give virtually identical quaternary structures with the same deviations from ideal 222 symmetry for all three resolution ranges.

The molecular envelope was remade from the symmetry-deviant model with partially rebuilt side chains. Density modification by improper noncrystallographic symmetry averaging (Vellieux & Read, 1995) was continued with resolution extension to 2.8 Å using the new molecular envelope. After ten more cycles of improper noncrystallographic density averaging at 2.8 Å, the remaining LmGAPDH residues, including the N-terminal Ala insertion, were built into the model according to the density of the averaged map. No density could be seen for the two C-terminal residues, Lys-359 and Met-360, so these two residues were deleted from the model. During the density modification, no phase combination was carried out, and no map inversion amplitudes and phases were used for missing data.

The model containing the correct LmGAPDH residues 1−358 for each of the four subunits was refined by simulated annealing with noncrystallographic symmetry restraints followed by B-factor refinement, which lowered the R_{factor} to

0.236. The noncrystallographic symmetry restraints were then removed, and the model was further refined by Powell minimization and *B*-factor refinement, resulting in an R_{factor} of 0.213. At this point, the NAD^+s, which had been used in the generation of the molecular envelope for density modification but had not been included in model refinements, were rebuilt into each of the subunits according to the unequivocal density for the dinucleotides in the 2.8 Å averaged map. In addition, two inorganic phosphates were built into each of the four subunits according to the density of this map. The LmGAPDH tetramer model with four NAD^+s and eight phosphates was then refined by Powell minimization and *B*-factor refinement without noncrystallographic symmetry restraints to a final R_{factor} of 0.198. No waters were built into the model. All model refinements were executed with X-PLOR (Brünger, 1992). All interactive model building was executed with O (Jones *et al.*, 1991).

Modeling of the Hemithioacetal Reaction Intermediate. The tetrahedral hemithioacetal intermediate of the GAPDH reaction was modeled into the structure of LmGAPDH in two different conformations, one with its 3-phosphate moiety in the substrate phosphate (P_s) binding site and the other with its 3-phosphate in the inorganic phosphate (P_i) binding site. The intermediate was also modeled into the structure of TbGAPDH with its 3-phosphate moiety in the P_i binding site of TbGAPDH. All modeling was executed with the BIOGRAF 3.21 package (Molecular Simulations, Inc., Burlington, MA) in conjunction with the DREIDING-II force field (Mayo *et al.*, 1990). The hemithioacetal positioning was subjected to weak harmonic distance restraints (force constant = 30 kcal mol^{-1} $Å^{-2}$), forcing the phosphorus atom of the intermediate into either the P_s or P_i position. The final models were obtained by conjugate gradient minimization to convergence of the Cys−hemithioacetal adduct (Cys-166 in LmGAPDH, Cys-165 in TbGAPDH) with all other residues and the NAD^+ kept fixed in their crystallographically determined positions.

RESULTS

The final refined model of the LmGAPDH tetramer contains residues 1−358, one NAD^+, and two inorganic phosphates for each of the four subunits. For the protein portion, the rms deviations from ideality are 0.013 Å for bond lengths and 3.09° for bond angles. Energetically favorable conformations predominate in the protein (Figure 2). In each of the four subunits, the residue deviating most from an allowed region of the Ramachandran plot is Val-255, which occurs in a turn connecting two β-strands about 10 Å from the active site. This residue is conserved in GAPDHs from *T. brucei*, human, *Bacillus stearothermophilus*, and lobster (Vellieux *et al.*, 1993; Watson *et al.*, 1972; Skarżyński *et al.*, 1987; Moras *et al.*, 1975). In the structures of these four GAPDHs, this Val is also in the same region of the Ramachandran plot as in LmGAPDH. The similar ϕ,ψ values for this residue in all of these GAPDH structures indicate that this is a characteristic structural feature of GAPDHs and not a peculiarity in the LmGAPDH model. The recently determined structure of *Thermotoga maritima* GAPDH shows the same backbone conformation in this region, but the residue corresponding to Val-255 in LmGAPDH has been substituted by Gly (Korndörfer *et al.*, 1995).

Although the final rounds of refinement employed no noncrystallographic symmetry restraints, the conformations

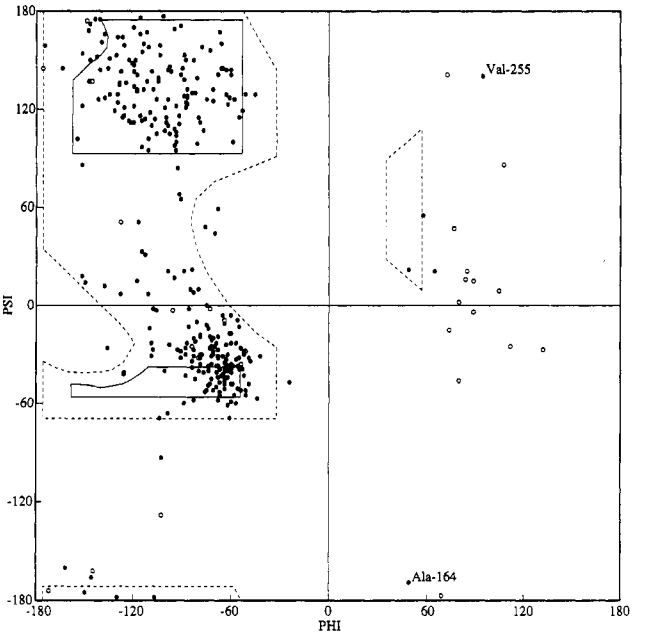

FIGURE 2: Ramachandran plot for a subunit of the final refined LmGAPDH tetramer. Hollow circles represent Gly. All other amino acids are represented by filled circles.

Table 1: rms Deviations of Subunits of Trypanosomal GAPDHs from *L. mexicana* GAPDH Subunit A after Backbone Superposition (Å)

	LmGAPDH			TbGAPDH
	subunit B	subunit C	subunit D	subunit A
backbone	0.27	0.27	0.26	0.59
NAD^+	0.35	0.33	0.42	0.35

of all four subunits in the final refined tetramer are very similar. Using the A subunit as a reference, the rms deviations of backbone atoms (N, C^α, C) after superposition of the B, C, and D subunits are less than 0.3 Å for each superposition. Likewise, the conformations of the bound NAD^+s are very similar as superpositions of the NAD^+s from the B, C, and D subunits onto the A subunit NAD^+ result in rms deviations of less than 0.4 Å for each superposition (Table 1).

There are slight deviations of less than 0.5° from ideal 222 molecular symmetry in the final refined tetramer. There is no single perfect molecular 2-fold axis as has been reported for human skeletal muscle holo-GAPDH (Mercer *et al.*, 1976) and *Bacillus coagulans* apo-GAPDH (no NAD^+ bound) (Griffith *et al.*, 1983). GAPDHs from some sources have shown cooperativity in the binding of NAD^+ (Conway & Koshland, 1968; De Vijlder *et al.*, 1969; Seydoux *et al.*, 1973). This apparent asymmetry in binding has been explained by modeling GAPDH as a dimer of dimers deviating from ideal 222 molecular symmetry (Bernhard & MacQuarrie, 1973; Moras *et al.*, 1975). In contrast, no cooperativity in cofactor binding has been seen in trypanosomatid GAPDHs (Lambeir *et al.*, 1991). The present structure was refined with full occupancies assigned to the four bound NAD^+s. The average *B*-factors of the atoms in each of the four NAD^+s are 40, 27, 34, and 31 $Å^2$, compared with the average *B*-factor of 31 $Å^2$ for the entire refined LmGAPDH tetramer model (including NAD^+s and phosphates) and 29 $Å^2$ for the backbone atoms only of the LmGAPDH tetramer. These *B*-factors indicate that all four

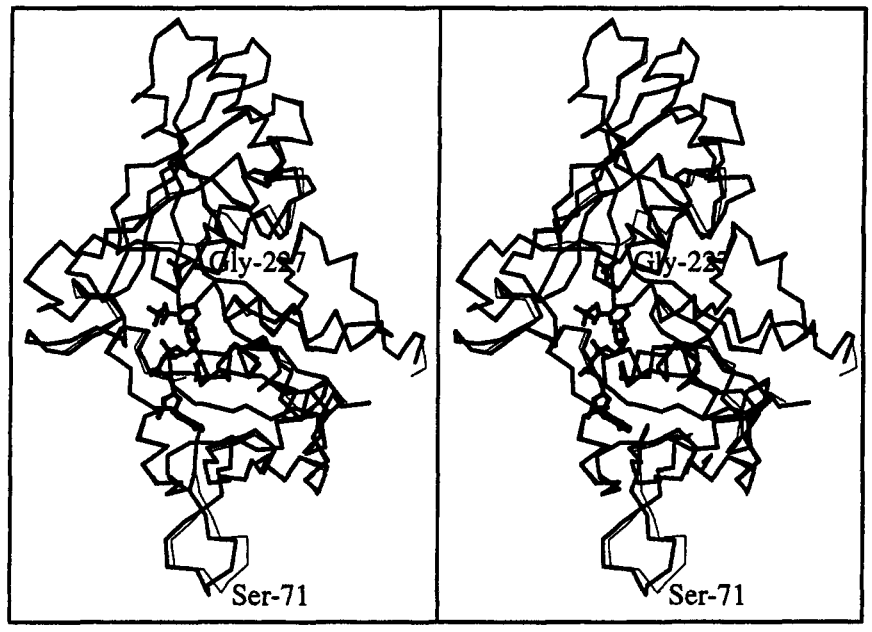

FIGURE 3: Stereoview of the superposition of the TbGAPDH C^{α} trace (thin lines) onto the LmGAPDH C^{α} trace (thick lines). The NAD^+ and the two inorganic phosphates in LmGAPDH are also shown. Ser-71 and Gly-227 are indicated to show the regions where the two structures deviate most. This figure was generated using MOLSCRIPT (Kraulis, 1991).

NAD^+ binding sites are essentially equally occupied and that the assumption of full occupancy for the NAD^+s was valid.

In general, the structure of LmGAPDH is very similar to that of TbGAPDH, as the overall rms deviation for backbone atoms between the two structures is 0.6 Å (Table 1). There are, however, two regions where the backbone atoms show relatively large rms deviations between these two structures (Figure 3). One region comprises residues Arg-58 through Glu-73 in LmGAPDH. This solvent-exposed region contains an eight-residue insertion which is characteristic of trypanosomatid glycosomal GAPDHs (Hannaert *et al.*, 1992). The rms deviation in backbone atoms in this region between LmGAPDH and TbGAPDH is 1.7 Å. The other region of large backbone deviations between the two structures spans residues Ser-224 through Ala-228 in LmGAPDH. The rms deviation in backbone atoms in this region between the two structures is 1.9 Å. The largest deviation in this region, of 3.5 Å, occurs between C^{α} of Gly-227 in LmGAPDH and the corresponding C^{α} of Gly-226 in TbGAPDH. $F_o - F_c$ electron density maps clearly indicated the conformation of this loop in LmGAPDH (Figure 4a).

Two inorganic phosphates were built into each of the subunits in the final model (Figure 4b). The phosphates were assigned full occupancy during the refinement, and the average *B*-factor of the atoms in the eight phosphates is 37 $Å^2$. The phosphate in the inorganic site (P_i) is bound by the O^{γ}s of Ser-165, Thr-167, and Thr-226 and the backbone amide N of Gly-227. The phosphate in the substrate site (P_s) is bound by the O^{γ}s of Thr-197 and Thr-199, the guanidinium Ns of Arg-249, and the nicotinamide O2′ ribose hydroxyl of the NAD^+ (Figure 5a). The presence of the two phosphates in LmGAPDH contrasts with previous GAPDH structures, including TbGAPDH, which contained two bound sulfates (Figure 5b; Vellieux *et al.*, 1993; Skarżyński & Wonacott, 1988; Skarżyński *et al.*, 1987; Moras *et al.*, 1975; R. J. Read, 1993, unpublished results; Korndörfer *et al.*, 1995).

One of the two phosphates in the LmGAPDH structure occupies the putative P_s binding site as seen in all previous GAPDH structures. Quite remarkably, the other phosphate in LmGAPDH is not bound in the "classical P_i" site of previous GAPDH structures. Due to their high amino acid sequence identity, the difference in phosphate binding site positions between the closely related trypanosomatid GAPDHs is especially interesting. Upon superposition of the TbGAPDH backbone onto the LmGAPDH backbone, the deviation in position between the phosphorus atom of the phosphate in the P_s site of LmGAPDH and the sulfur atom of the sulfate in the P_s site of TbGAPDH is less than 0.1 Å. At the same time, the deviation of the position between the phosphorus atom of the P_i phosphate in LmGAPDH and the sulfur atom of the P_i sulfate in TbGAPDH is 2.9 Å (Figure 6). The repositioning of the P_i anion binding site in LmGAPDH is necessary to accommodate the aforementioned difference in the conformation of the loop spanning residues Ser-224 through Ala-228 (Figure 6). The positions of the corresponding phosphate binding sites are well conserved among the four subunits of LmGAPDH. Upon superposition of the backbones of the B, C, and D subunits onto the backbone of the A subunit, the deviations in the positions of the phosphorus atoms of the phosphates within each of the two sites are less than 0.4 Å.

DISCUSSION

LmGAPDH and Drug Design. The present work is part of our continuing structure-based design of trypanocidal compounds which may lead to effective drug therapies in the treatment of diseases caused by trypanosomatids. By turning our attention to LmGAPDH, which is 81% identical in amino acid sequence to TbGAPDH (Hannaert *et al.*, 1992), we have circumvented some of the potential major obstacles in the structure-based drug design strategy targeted at trypanosomatid GAPDH. The overexpression system for LmGAPDH (Hannaert *et al.*, 1994) now provides an ample supply of pure trypanosomatid GAPDH. For the present study, enough LmGAPDH was obtained from 2 L of cell culture to allow the screening of over 1200 crystallization conditions based on the crystallization matrices developed in our laboratory (S. Sarfaty, F. van den Akker, and W. G. J. Hol, 1994, unpublished results). The LmGAPDH crystals

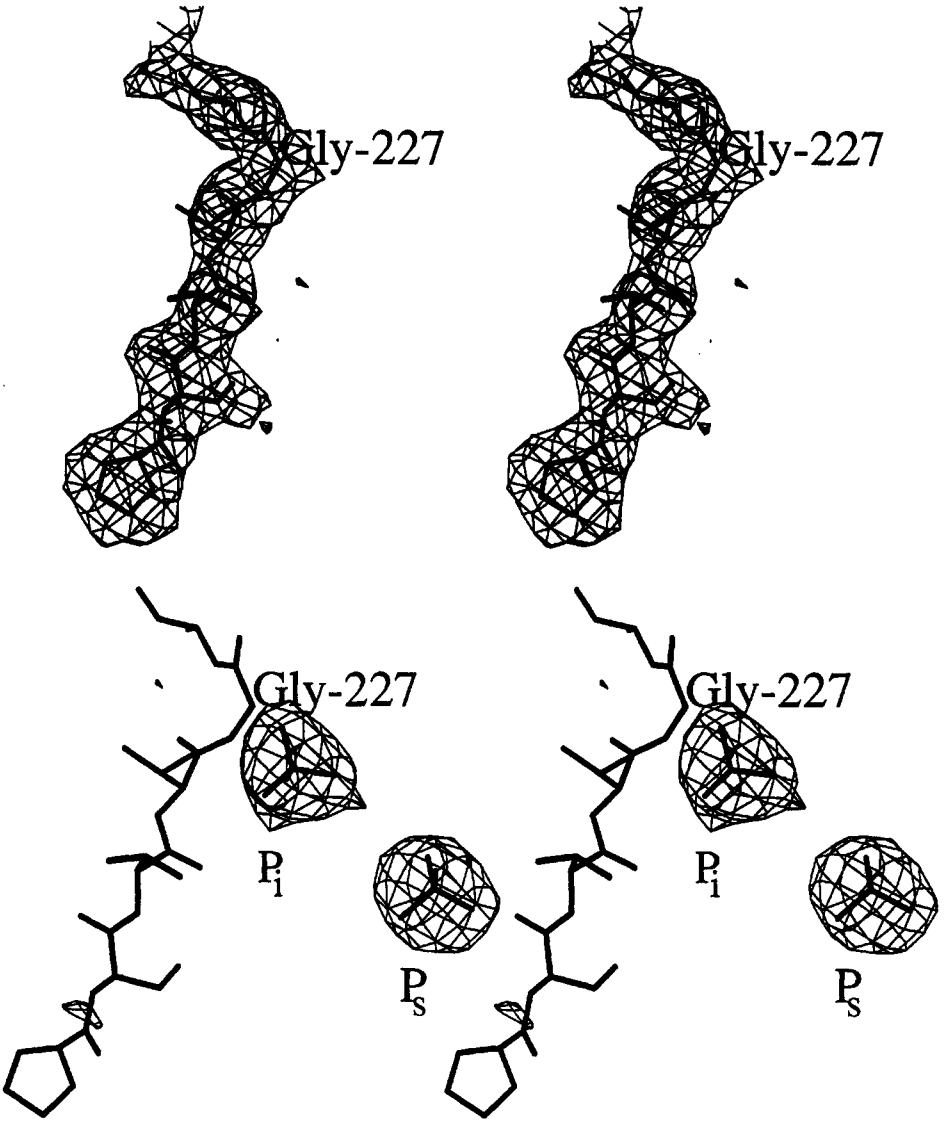

FIGURE 4: (a, top) Stereoview of the electron density associated with Pro-223−Ala-228 in subunit A of LmGAPDH. The electron density is from an $F_o - F_c$ map in which Pro-223−Ala-228 were omitted from the structure factor calculations. The contour level is 2σ. The coordinates of Pro-223−Ala-228 are shown superimposed onto the electron density. (b, bottom) Stereoview of the electron density associated with the bound phosphates in subunit A of LmGAPDH. The electron density is from an $F_o - F_c$ map in which the phosphates were omitted from the structure factor calculations. The contour level is 3σ. The coordinates of the phosphates and Pro-223−Ala-228 are shown superimposed onto the electron density.

were eventually grown from conditions entirely different from the crystallization conditions for TbGAPDH crystals (Read *et al.*, 1987). Crystal lifetime in the X-ray beam has also proven to be a major advantage of working with LmGAPDH instead of TbGAPDH. All of the data used in the determination of the present structure were collected from a single crystal without the aid of cryocooling. Furthermore, a 90% complete data set to 3.0 Å resolution with an R_{sym} of 0.069 has recently been collected from a single LmGAPDH crystal using an in-house Rigaku RU-200 generator and an R-AXIS II area detector (H. Kim and W. G. J., Hol, 1994, unpublished results). Thus, it appears that further structural studies toward trypanocidal GAPDH inhibitors may not have to absolutely depend on the availability of synchrotron radiation.

Consistent with their high amino acid sequence identity, the structures of LmGAPDH and TbGAPDH are very similar (Figure 3). Furthermore, the structural similarities extend to the binding modes of the NAD^+ cofactors which adopt practically identical conformations in the binding sites of these isozymes (Table 1, Figure 6). The similarities in the NAD^+ binding modes in LmGAPDH and TbGAPDH and the very high degree of sequence identity in the NAD^+ binding grooves among various trypanosomatid GAPDHs suggest that inhibitor designs based on the NAD^+ binding mode of a particular trypanosomatid GAPDH will be applicable to GAPDHs from other trypanosomatids. Adenosine derivative GAPDH inhibitors have been designed which exploit structural differences between trypanosomatid and human GAPDHs to selectively inhibit the trypanosomatid isozyme. Although these inhibitors were designed with respect to the NAD^+ binding mode in TbGAPDH, they showed similar inhibition constants for LmGAPDH (Verlinde *et al.*, 1994b).

There are, however, certain structural differences among glycosomal GAPDHs from various trypanosomatids which may contribute to some differences in inhibitor binding between the various isozymes. The best inhibitor from the aforementioned study of adenosine-based compounds was the 2′-*m*-methoxybenzamido derivative of adenosine (MBDA; Verlinde *et al.*, 1994b). The apparent affinity of this compound for LmGAPDH is almost an order of magnitude

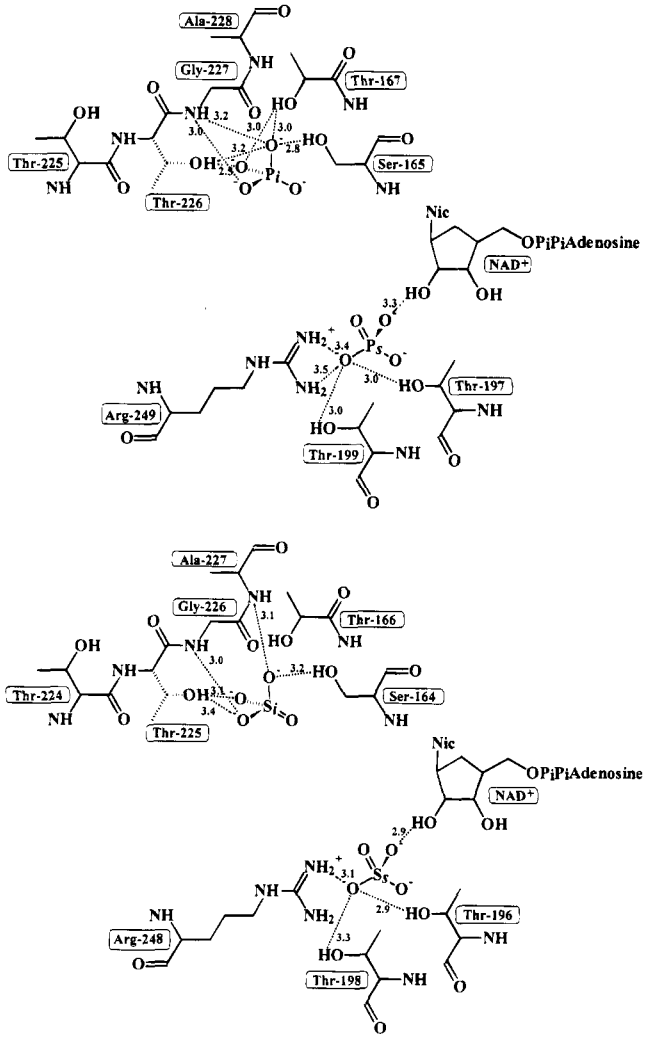

FIGURE 5: Schematic diagrams of the phosphate binding sites in LmGAPDH (a, top) and the sulfate binding sites in TbGAPDH (b, bottom). The inorganic and substrate anion binding sites are denoted by subscripts i and s, respectively. Selected interactions shorter than 3.5 Å are indicated. LmGAPDH contains the "new" P_i site, and TbGAPDH contains the "classical" P_i site. Although the phosphate is depicted as PO_4^{3-} in (a), the amphiprotic nature of the Ser and Thr side chains could well accommodate HPO_4^{2-}, which is likely the predominant protonation state of phosphate at pH 7. All of the anion binding residues shown are strictly conserved between LmGAPDH and TbGAPDH.

greater than for TbGAPDH. At the same time, the closely related 2′-benzamido derivative of adenosine shows only a 2-fold greater affinity for LmGAPDH than for TbGAPDH. It appears that the additional *m*-methoxy moiety of MBDA is large enough to probe regions of the NAD^+ binding groove which are not strictly conserved between LmGAPDH and TbGAPDH. The modeled binding mode of MBDA in TbGAPDH shows the methoxy O of the inhibitor interacting with the $N^{\delta 2}$ of Asn-39 (Figure 7). At first glance, this modeled interaction may appear to be a weakly stabilizing hydrogen bond. The analogous residue in LmGAPDH is Ser-40. The conformation of this side chain is such that the O^{γ} is hydrogen bonded to the backbone amides of Thr-41 and Asn-42. Because of this intraprotein interaction, the modeled binding mode of MBDA in LmGAPDH shows no interaction between the inhibitor and Ser-40. Yet, the LmGAPDH−MBDA complex appears to be more stable than the TbGAPDH−MBDA complex which, due to Asn-39, has been modeled to have more protein−inhibitor interactions (Figure 7).

A possible explanation for the apparent greater affinity of MBDA for LmGAPDH than for TbGAPDH may lie in the differences in solvation between the free inhibitor and the enzyme−inhibitor complex for the two isozymes. In the situation of free inhibitor, the methoxy O of MBDA is likely bound to one or two waters. In the absence of ligand, Ser-40 in LmGAPDH and Asn-39 in TbGAPDH are also likely bound to waters since these residues are at the enzyme surface. It may be that, in order to make the Asn-39 $N^{\delta 2}$−methoxy O protein−inhibitor interaction in the TbGAPDH−MBDA complex, a more favorable Asn-39 $N^{\delta 2}$−water interaction must be displaced. Since Ser-40 of LmGAPDH does not participate in any interactions with the inhibitor in the modeled LmGAPDH−MBDA complex, a favorable solvation of Ser-40 in the free enzyme state may be retained even upon inhibitor binding. Hence, differences in solvent structure of the TbGAPDH− and LmGAPDH−inhibitor complexes might be responsible for the observed differences in MBDA affinity.

It is unlikely that the difference in affinity of MBDA for LmGAPDH and TbGAPDH is due in significant part to conformational differences in residues other than the aforementioned serine and asparagine. The protein residues within 4 Å of MBDA in the modeled LmGAPDH−MBDA complex are Asn-8, Phe-10, Gly-11, Asp-38, Met-39, Ala-90, Gln-91, Thr-111, and Leu-113. These residues are strictly conserved between LmGAPDH and TbGAPDH. The rms deviation in backbone atoms for these residues between LmGAPDH and TbGAPDH is 0.2 Å, and the rms deviation for the side-chain atoms is 0.5 Å (cf. Table 1). Certainly, the structural basis for the differences in MBDA binding to LmGAPDH and TbGAPDH will be fully revealed only upon the determinations of the structures of the respective complexes.

The great structural similarities in the binding of NAD^+ and the conformations of the NAD^+-binding residues between LmGAPDH and TbGAPDH are reassuring for further structure-based drug design. The implications from kinetic and structural studies are that the current strategy of designing adenosine-derived GAPDH inhibitors based on the structure of one trypanosomatid GAPDH (Verlinde *et al.*, 1994b) may result in compounds which are effective against GAPDHs from many trypanosomatid species. That this should be the case is not entirely surprising in light of the evolutionary conservation of GAPDH. A common ancestor of *Leishmania* and *Trypanosoma* presumably occurred over 400 million years ago, and yet, their GAPDHs are still over 80% identical in sequence (Hannaert *et al.*, 1992; P. A. M. Michels, 1994, personal communication).

Substrate Binding in GAPDH. The conformation of the loop spanning residues Ser-224 through Ala-228 in the catalytic domain of LmGAPDH is different from the corresponding regions in TbGAPDH and nearly all previous structures of GAPDHs (Vellieux *et al.*, 1993; Watson *et al.*, 1972; Moras *et al.*, 1975; Skarżyński *et al.*, 1987). This region of the protein is at the edge of a β-sheet in the active site. Compared with most previous GAPDH structures, the conformation of this stretch in LmGAPDH is such that it constricts the active site of LmGAPDH, effectively excluding anion binding in the classical P_i site, seen in the structures of GAPDHs from lobster, human, *T. brucei*, and *B. stearo-*

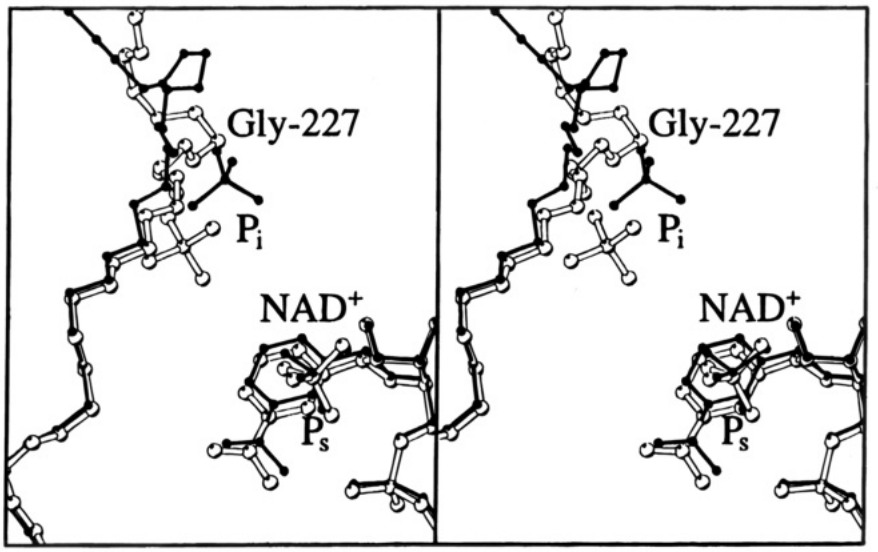

FIGURE 6: Stereoview of the backbone atoms of the Ser-224−Ala-228 loop in LmGAPDH (hollow) and the corresponding region in TbGAPDH (solid), plus the two bound phosphates in LmGAPDH and the two bound sulfates in TbGAPDH and the NAD^+s in both LmGAPDH and TbGAPDH after superposition of TbGAPDH onto LmGAPDH. LmGAPDH contains the "new P_i" site, and TbGAPDH contains the "classical P_i" site. This figure was generated using MOLSCRIPT (Kraulis, 1991).

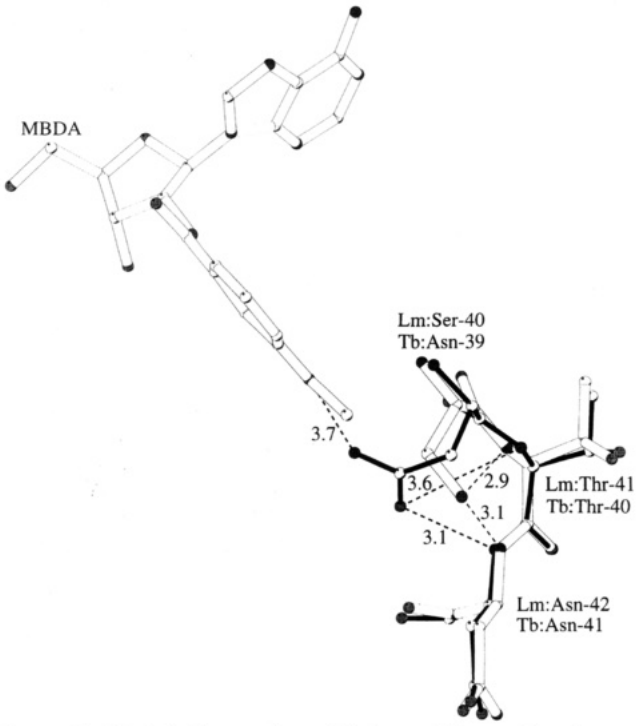

FIGURE 7: Modeled interaction of 2′-deoxy-2′-(*m*-methoxybenzamido)adenosine (MBDA) with the residue in the NAD^+ binding region which is not conserved between LmGAPDH and TbGAPDH. The conformations of the protein residues shown are crystallographically determined. Protein residues of LmGAPDH are drawn in thick hollow bonds, and those of TbGAPDH are drawn in thin solid bonds. Selected distances in angstroms are drawn in dashed lines. Oxygens and nitrogens are shaded. This figure was generated using MOLSCRIPT (Kraulis, 1991).

thermophilus (Figure 8a; Moras *et al.*, 1975; Watson *et al.*, 1972; Vellieux *et al.*, 1993; Skarżyński *et al.*, 1987). Upon superposition of the TbGAPDH protein backbone onto the LmGAPDH protein backbone, the P_i sulfate of TbGAPDH assumes a position which is too close to the backbone atoms of LmGAPDH. The superimposed P_i sulfate of TbGAPDH is only 1.0 Å from the backbone atoms of Gly-227 in LmGAPDH. There is no such unfavorable steric clash in LmGAPDH as the "new P_i" anion binding site in LmGAPDH is shifted ~3 Å from the classical P_i binding site (Figure 6).

Among previous GAPDH structures, only the recent structure of GAPDH from thermophilic *T. maritima* (TmGAPDH; Korndörfer *et al.*, 1995) shows the same conformation of the 224−228 (LmGAPDH numbering) loop and repositioning of the P_i binding site as seen in LmGAPDH (Figure 8b). This conformation is certainly not due to primary structure peculiarities in LmGAPDH and TmGAPDH. The amino acid sequence for this region in LmGAPDH is highly conserved in the structurally equivalent regions in GAPDHs from *T. brucei*, *B. stearothermophilus*, lobster, human, and *T. maritima* (Figure 9). Crystal packing also does not appear to be a factor inducing this conformation. In the LmGAPDH crystal lattice, there are no residues of crystallographically related mates within 5 Å of this loop. The *B*-factors in this region of the protein, albeit, are higher than the average *B*-factor for the entire structure, indicating greater-than-average flexibility in this loop, compared with the entire structure. The average backbone *B*-factor of Gly-227 is 45 $Å^2$, compared with an average backbone *B*-factor of 31 $Å^2$ for the entire structure. Nevertheless, it is most likely that this region in the LmGAPDH structure has been built correctly. Model refinement without noncrystallographic symmetry restraints converged to give this conformation in all four crystallographically independent subunits of the LmGAPDH tetramer. The rms deviations in backbone atoms in residues 223−228 between the A subunit and any of the other three subunits after C^α superpositions of the entire polypeptide chains range from 0.14 to 0.23 Å. Furthermore, the electron density for this region is clearly traceable (Figure 5a).

This unusual conformation of Ser-224 through Ala-228 in LmGAPDH should now be considered in the analyses of substrate binding and the catalytic mechanism of GAPDH. Two phosphates are involved in the oxidative phosphorylation of glyceraldehyde 3-phosphate (GAP) to 1,3-bis-(phosphoglycerate) (BPG) catalyzed by GAPDH. One phosphate, the substrate phosphate (P_s), is the 3-phosphate of GAP. The other phosphate, the inorganic phosphate (P_i), executes the phosphorolysis of the covalent thioester intermediate adduct involving the essential cysteine to release the product BPG [Figure 1; for a review of the mechanism,

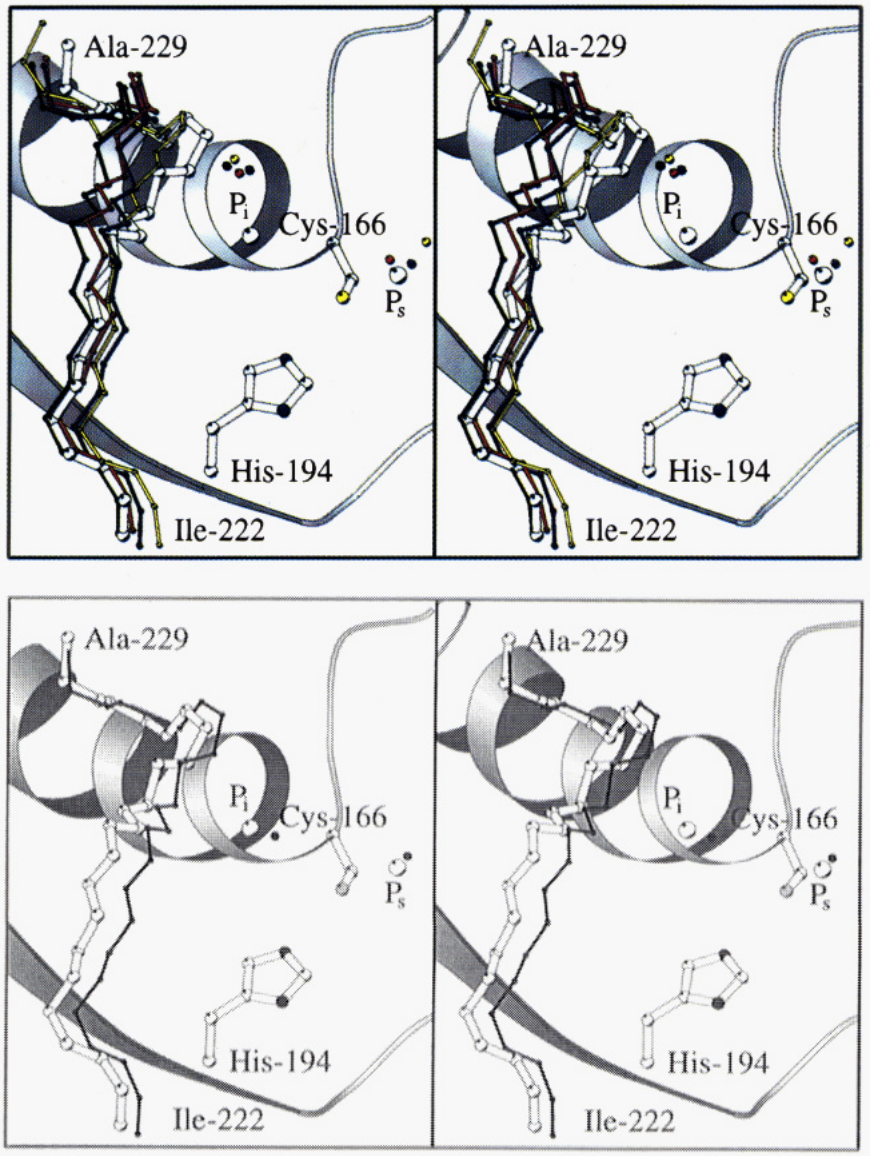

FIGURE 8: Stereoviews of the phosphate binding site environment in the active sites of GAPDHs. Shown in white are the backbone atoms of the stretch spanning Ile-222−Ala-229 in LmGAPDH, the phosphorus positions of the two bound phosphates in LmGAPDH, and the catalytic Cys and His in LmGAPDH. The secondary structure in LmGAPDH in this region is also shown. (a, top) The protein stretch corresponding to LmGAPDH Ile-222−Ala-229 and the positions of the sulfur atoms of the bound sulfates in TbGAPDH (black), BsGAPDH (blue), human GAPDH (red), and lobster GAPDH (yellow) are shown after superposition of their respective backbones onto the LmGAPDH backbone. The S^{γ} of Cys-166 is drawn in yellow, and the imidazole Ns of His-194 are drawn in blue. Note the deviation in position of the P_i phosphate in LmGAPDH from the P_i sulfates in the other GAPDHs resulting from the different conformation of the Ile-222−Ala-229 stretch in LmGAPDH. (b, bottom) The protein stretch corresponding to Ile-222−Ala-229 in TmGAPDH (black) and the positions of the sulfur atoms of the bound sulfates are shown after superposition of the TmGAPDH backbone onto the LmGAPDH backbone. Note the similarity between the loop conformations in these two structures, compared with the other GAPDHs shown in (a). The P_i positions in LmGAPDH and TmGAPDH differ by 0.9 Å. This figure was generated using MOLSCRIPT (Kraulis, 1991).

L. mex.	221IIPSTTGAA229
T. brucei	220.....228
B. stear.	204...T.....212
lobster	202....S....210
human	205...AS....213
T. marit.	203...T.....211

FIGURE 9: Sequence alignment of the protein stretch whose conformation is different in LmGAPDH compared with previous GAPDH structures. Conserved residues are indicated by dots. Shown are GAPDH sequences from *L. mexicana*, *T. brucei*, *B. stearothermophilus*, lobster, human, and *T. maritima*.

see Harris and Waters (1976)]. From previous GAPDH structures, the two putative phosphate binding sites were located by the identification of two bound sulfates. The binding of sulfates seen in the previous GAPDH structures was most likely due to the high concentration of ammonium sulfate (~2 M) from which the GAPDH crystals were grown (Buehner *et al.*, 1974; Skarżyński *et al.*, 1987; Read *et al.*, 1987). In contrast, the bound anions in LmGAPDH are phosphates as the crystals were grown from a relatively low concentration 200 mM phosphate-buffered PEG-1000 solution which contained no sulfate (see Materials and Methods). The phosphate concentration of the LmGAPDH crystallization medium is probably a more accurate reflection of the ~0.05 M phosphate concentration in cells (Brock *et al.*, 1984) than are the much higher sulfate concentrations from which previous GAPDH crystals were grown. Considering these differences between the crystallization environments of LmGAPDH and most previous GAPDHs, the conformation of residues Ser-224 through Ala-228 in LmGAPDH, and the concomitant repositioning of the P_i anion binding site,

may be more physiological than those seen in most previous GAPDH structures.

Although the two anion binding sites in GAPDH have historically been designated as "substrate" and "inorganic", some studies have indicated that the functional roles of these binding sites may be less discrete than once believed. The substrate analogue glycidol 3-phosphate was reported to bind in *B. stearothermophilus* GAPDH (BsGAPDH) with its 3-phosphate in the P_i site, indicating that the inorganic phosphate binding site may be involved to some extent in substrate binding (Skarżyński *et al.*, 1987). A more recent mutagenesis study of BsGAPDH also proposes that the substrate initially binds with its 3-phosphate in the P_i site (Corbier *et al.*, 1994). After formation of the hemithioacetal intermediate adduct with the essential Cys, the intermediate is proposed to flip to the P_s site.

To investigate the plausibility of substrate binding in the anion binding sites, in light of our new results, three models of the hemithioacetal intermediate of the reaction were built (Figure 10). First, the intermediate was modeled into LmGAPDH with its 3-phosphate group in the P_s site, which is well conserved among all GAPDH structures (Figure 10a). Second, the intermediate was modeled into LmGAPDH with its 3-phosphate group in the repositioned new P_i site (Figure 10b). Third, the intermediate was modeled into TbGAPDH with its 3-phosphate group in the classical P_i site (Figure 10c). In all three models, the hemithioacetal adduct is free of energetically prohibitive contacts with the protein.[3,4]

There are important differences among these three modeled conformations of the hemithioacetal intermediate. The first difference concerns the distance between the hemithioacetal and the nicotinamide ring of the NAD^+. The distances between the C1 carbon of the hemithioacetal and the C4 carbon of the nicotinamide ring are 2.9, 3.1, and 4.2 Å, respectively, in the P_s, new P_i, and classical P_i conformations of the hemithioacetal (Figure 10). Since there is a hydride transfer between these two atoms in the GAPDH reaction, a shorter C1−C4 distance would be more conducive for the reaction to occur. Thus, concerning the hydride transfer aspect of the GAPDH reaction, the classical P_i conformation of the hemithioacetal (Figure 10c) is the least favorable among the three modeled conformations.

The classical P_i conformation of the hemithioacetal (Figure 10c) also appears least favorable among the three modeled conformations when the position of the catalytically important His is taken into consideration (His-194 in LmGAPDH, His-193 in TbGAPDH). It has been proposed that the active site His functions in part as a hydrogen bond donor, via its N^ϵ, facilitating the formation of tetrahedral intermediates (Soukri *et al.*, 1989). In the P_s conformation, the distance between the C1 hydroxyl oxygen of the hemithioacetal and the N^ϵ of the active site His is 2.9 Å (Figure 10a). In the new P_i conformation (Figure 10b), this distance is 3.3 Å, and in the classical P_i conformation (Figure 10c), this distance is 5.0 Å. Thus, with respect to the position of the catalytically important His, the classical P_i conformation of the hemithioacetal again appears to be the least favorable among the three modeled conformations.

Next, it is interesting to consider the two remaining conformations of the intermediate, P_s and new P_i (Figure 10a,b), from the perspective of phosphorolysis. In the GAPDH reaction, an inorganic phosphate executes a phosphorolytic nucleophilic attack on the thioester intermediate (Figure 1). Although it is the hemithioacetal intermediate which has been modeled, it is assumed that the conformation of the thioester remains largely unchanged from that of the hemithioacetal. The only structural difference between the hemithioacetal and the thioester is that the tetrahedral hydroxyl-bearing C1 of the hemithioacetal becomes a trigonal planar carbonyl in the thioester. A very favorable arrangement for phosphorolysis is achieved when the thioester is in the P_s conformation and the inorganic phosphate is in the new P_i site (Figure 10a). In this conformation, the nucleophilic phosphate oxygen is 3.1 Å from the C1 carbonyl carbon of the thioester and is well positioned for back-side nucleophilic attack on the carbonyl. In the other situation, when the thioester is in the new P_i conformation and the inorganic phosphate is in the P_s site (Figure 10b), the nucleophilic phosphate oxygen is 4.3 Å from the C1 carbonyl carbon of the thioester. Furthermore, the sharper angle defined by the phosphate oxygen and the carbonyl bond is less favorable for nucleophilic attack, and the path of nucleophilic attack is obstructed by the C2 hydroxyl moiety of the intermediate. Hence, the most favorable situation for phosphorolysis is to have the thioester intermediate in the P_s conformation and the inorganic phosphate in the new P_i site (Figure 10a).

There remains still the possibility that the substrate GAP initially binds in the new P_i site and subsequently flips to the P_s site after formation of the hemithioacetal intermediate (Corbier *et al.*, 1994). Our models show that the P_s conformation of the hemithioacetal is in an energetically favorable staggered conformation, but in the new P_i conformation, the intermediate is in a more energetically strained eclipsed conformation (Figure 10a,b). Hence, by conformational energetic considerations, disregarding the chemical aspects of the reaction, the P_s conformation of the intermediate appears to be more plausible than the new P_i conformation.

From these modeling studies on LmGAPDH and TbGAPDH, it appears that the P_s site in GAPDH is truly the substrate binding site, and there appear to be no structural features which would favor the substrate GAP and the subsequent hemithioacetal and thioester intermediates to bind in the P_i site. In addition, the LmGAPDH structure casts doubt on the physiological relevance of the classical P_i site, primarily due to three points: (i) LmGAPDH was crystallized from a solution which was buffered by phosphate, the true substrate in the GAPDH-catalyzed reaction, (ii) the 200 mM phosphate concentration from which LmGAPDH was crystallized is closer to the physiological 50 mM phosphate concentration in cells than are the much higher sulfate concentrations from which previous GAPDHs were crystallized, and (iii) modeling studies indicate that the repositioned P_i phosphate in LmGAPDH would be well positioned for phosphorolytic attack on the thioester intermediate of the reaction. The recently determined TmGAPDH structure also

[3] Contrary to what has been reported for BsGAPDH (Skarżyński *et al.*, 1987), a stereochemically reasonable model of the hemithioacetal intermediate with its 3-phosphate in the P_s site can be built into LmGAPDH.

[4] Another hypothetical arrangement of the hemithioacetal intermediate and the inorganic phosphate is to build the hemithioacetal intermediate into either the classical or new P_i site and place the inorganic phosphate into the other P_i site. This situation, however, is not possible for LmGAPDH as the conformation of the 224−228 loop blocks the classical P_i site. In TbGAPDH, this modeling would be rather implausible due to potential prohibitive van der Waals interactions between the inorganic phosphate and the 3-phosphate of the intermediate.

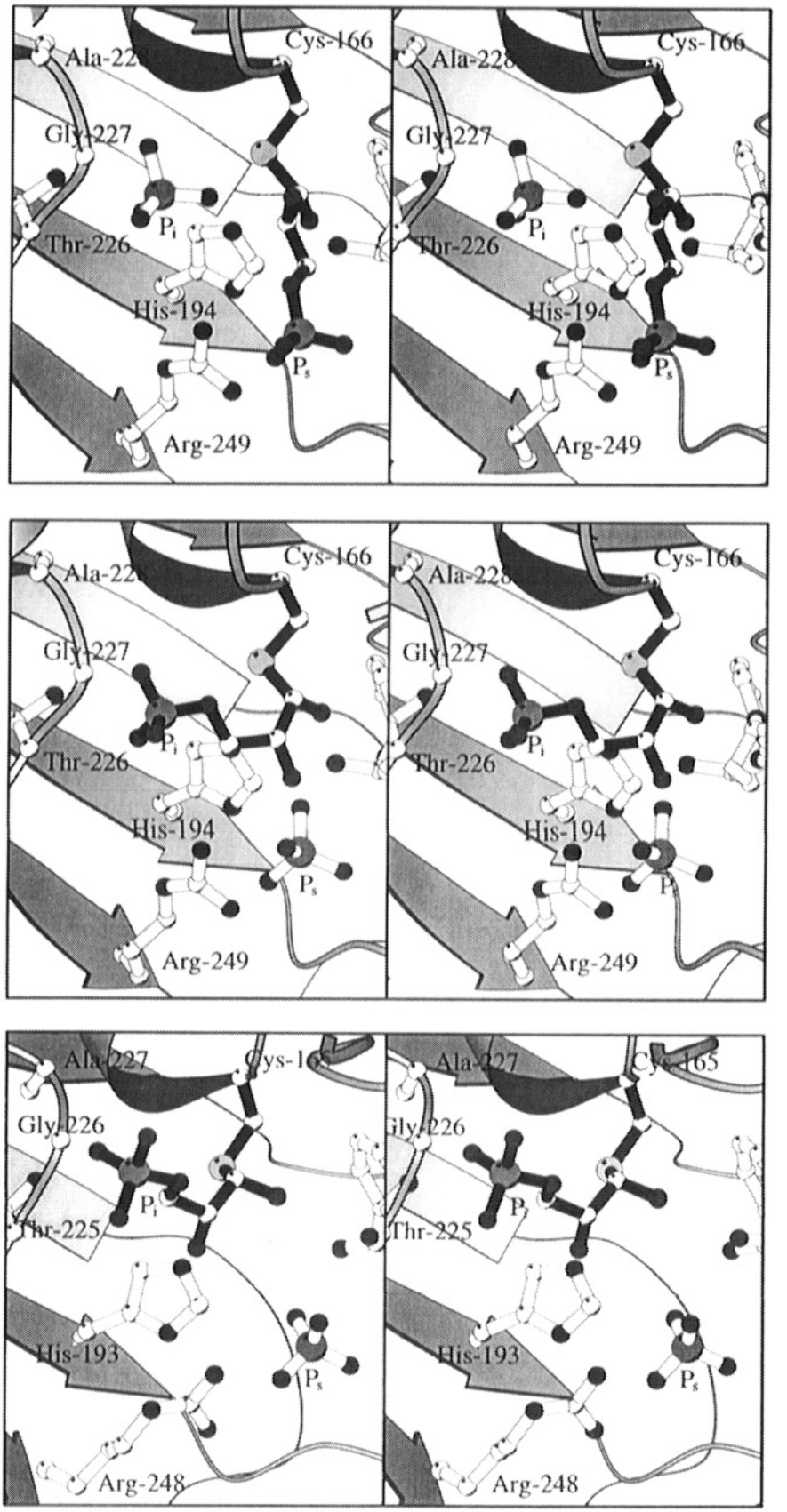

FIGURE 10: Stereoviews of the modeled hemithioacetal intermediate of the GAPDH reaction. The hemithioacetal is drawn in black bonds. Phosphorus, oxygen, nitrogen, and sulfur atoms are shaded. (a, top) The hemithioacetal modeled with its 3-phosphate group in the P_s site in LmGAPDH. This is the "P_s" conformation of the hemithioacetal. The inorganic phosphate shown occupies the new P_i site in LmGAPDH. (b, middle) The hemithioacetal intermediate modeled with its 3-phosphate group in the new P_i site in LmGAPDH. This is the "new P_i" conformation of the intermediate. (c, bottom) The hemithioacetal modeled with its 3-phosphate group in the classical P_i site in TbGAPDH. This is the "classical P_i" conformation of the intermediate.

shows the same conformation of the 224−228 loop as is observed in the LmGAPDH structure and a repositioning of the P_i sulfate from the classical P_i site (Figure 8b; Korndörfer *et al.*, 1995). These similarities between the structures of LmGAPDH and TmGAPDH may be due to a feature of TmGAPDH which favors the "low ionic strength" conforma-

tion of the 224−228 loop even at the rather high ionic strength conditions of the TmGAPDH crystallization (Tomschy *et al.*, 1993; Korndörfer *et al.*, 1995). This might be a reflection of a decreased flexibility at room temperature of a very thermostable protein. Further characterization of the true binding mode of substrates in GAPDH will require structure determinations of GAPDH−substrate analogue complexes. Such structures may come from our future studies on LmGAPDH, which crystallizes under conditions near physiological phosphate concentration and pH.

ACKNOWLEDGMENT

We thank Drs. Paul A. M. Michels and Véronique Hannaert (International Institute of Cellular and Molecular Pathology, Brussels, Belgium) for excellent discussions and for providing the LmGAPDH-overproducing strain of *E. coli*. We thank Dr. Fred R. Opperdoes (International Institute of Cellular and Molecular Pathology, Brussels, Belgium) for critical reading of the manuscript. We also thank the staff at the Stanford Synchrotron Radiation Laboratory for helpful discussions on data collection.

REFERENCES

Bellofatto, V., Fairlamb, A., Henderson, G. B., & Cross, G. A. (1987) *Mol. Biochem. Parasitol. 25*, 227−238.
Bernhard & MacQuarrie (1973) *J. Mol. Biol. 74*, 73−78.
Brock, T. D., Smith, D. W., & Madigan, M. T. (1984) *Biology of Microorganisms*, p 503, Prentice-Hall, Inc., Englewood Cliffs, NJ.
Brünger, A. T. (1992) *X-PLOR, Version 3.1, A System for X-Ray Crystallography and NMR*, Yale University Press, New Haven, CT.
Buehner, M., Ford, G. C., Moras, D., Olsen, K. W., & Rossmann, M. G. (1974) *J. Mol. Biol. 90*, 25−49.
Clarkson, A. B., Jr., & Brohn, F. H. (1976) *Science 194*, 204−206.
Conway & Koshland (1968) *Biochemistry 7*, 4011−4022.
Corbier, C., Michels, S., Wonacott, A. J., & Branlant, G. (1994) *Biochemistry 33*, 3260−3265.
De Vijlder, J. J. M., Hilvers, A. G., Van Lis, J. M. J., & Slater, E. C. (1969) *Biochim. Biophys. Acta 191*, 221−228.
Fairlamb, A. H., Opperdoes, F. R., & Borst, P. (1977) *Nature 265*, 270−271.
Griffith, J. P., Lee, B., Murdock, A. L., & Amelunxen, R. E. (1983) *J. Mol. Biol. 169*, 963−974.
Grogl, M., Thomason, T. N., & Francke, E. D. (1991) *Am. J. Trop. Med. Hyg. 47*, 117−126.
Hannaert, V., Blaauw, M., Kohl, L., Allert, S., Opperdoes, F. R., & Michels, P. A. M. (1992) *Mol. Biochem. Parasitol. 55*, 115−126.
Hannaert, V., Callens, M., Opperdoes, F. R., & Michels, P. A. (1994) *Eur. J. Biochem. 225*, 143−149.
Harrigan, P. J., & Trentham, D. R. (1973) *Biochem. J. 135*, 695.
Harris, J. I., & Waters, M. (1976) in *The Enzymes* (Boyer, P. D., Ed.) 3rd ed., Vol. 13, pp 1−49, Academic Press, San Diego.
Jones, T. A., Zou, J. Y., Cowan, S. W., & Kjeldgaard, M. (1991) *Acta Crystallogr., Sect. A 46*, 110−119.
Kirchhoff, L. V. (1993) *N. Engl. J. Med. 329*, 639−644.
Kolberg, R. (1994) *Science 264*, 1859−1861.
Korndörfer, I., Steipe, B., Huber, R., Tomschy, A., & Jaenicke, R. (1995) *J. Mol. Biol. 246*, 511−521.
Kraulis, P. (1991) *J. Appl. Crystallogr. 24*, 924−950.
Kuzoe, F. A. S. (1993) *Acta Trop. 54*, 153−162.
Lambeir, A.-M., Loiseau, A. M., Kuntz, D. A., Vellieux, F. M., Michels, P. A. M., & Opperdoes, F. R. (1991) *Eur. J. Biochem. 198*, 429−435.
Laskowski, R. A., MacArthur, M. W., Moss, D. S., & Thornton, J. M. (1993) *J. Appl. Crystallogr. 26*, 283−291.
Maingon, R., Feliciangeli, D., Guzman, B., Rodriguez, N., Convit, J., Adamson, R., Chance, M., Petrlanda, I., Dougherty, M., & Ward, R. (1994) *Ann. Trop. Med. Parasitol. 88*, 29−36.
Mayo, S. L., Olafson, B. D., & Goddard, W. A., III (1990) *J. Phys. Chem. 94*, 8897−8909.
Mercer, W. D., Winn, S. I., & Watson, H. C. (1976) *J. Mol. Biol. 104*, 277−283.
Moras, D., Olsen, K. W., Sabesan, M. N., Buehner, M., Ford, G. C., & Rossmann, M. G. (1975) *J. Biol. Chem. 250*, 9137−9162.
Opperdoes, F. R. (1987) *Annu. Rev. Microbiol. 41*, 127−151.
Opperdoes, F. R., & Borst, P. (1977) *FEBS Lett. 80*, 360−364.
Polgár, L. (1975) *Eur. J. Biochem. 51*, 63−71.
Racker, E., & Krimsky, I. (1958) *Fed. Proc., Fed. Am. Soc. Exp. Biol. 17*, 1135.
Read, R. J. (1986) *Acta Crystallogr., Sect. A 42*, 140−149.
Read, R. J., Wierenga, R. K., Groendijk, H., Hol, W. G. J., Lambeir, A., & Opperdoes, F. R. (1987) *J. Mol. Biol. 194*, 573−575.
Segal, H. L., & Boyer, P. D. (1953) *J. Biol. Chem. 204*, 265.
Seydoux et al. (1973) *Biochemistry 12*, 4290−4300.
Sim, G. A. (1959) *Acta Crystallogr. 12*, 813−815.
Skarżyński, T., & Wonacott, A. J. (1988) *J. Mol. Biol. 203*, 1097−1118.
Skarżyński, T., Moody, P. C. E., & Wonacott, A. J. (1987) *J. Mol. Biol. 193*, 171−187.
Soukri, A., Mougin, A., Corbier, C., Wonacott, A., Branlant, C., & Branlant, G. (1989) *Biochemistry 28*, 2586−2592.
Tanowitz, H. B., Kirchhoff, L. V., Simon, D., Morris, S. A., Weiss, L. M., & Wittner, M. (1992) *Clin. Microbiol. Rev. 5*, 400−419.
Tomschy, A., Glockshuber, R., & Jaenicke, R. (1993) *Eur. J. Biochem. 214*, 43−50.
Veeken, H. J. G. M., Ebeling, M. C. A., & Dolmans, W. M. V. (1989) *Trop. Geogr. Med. 41*, 113−117.
Vellieux, F. M. D., & Read, R. J. (1995) *J. Appl. Crystallogr.* (submitted for publication).
Vellieux, F. M. D., Hajdu, J., Verlinde, C. L. M. J., Groendijk, H., Read, R. J., Greenhough, T. J., Campbell, J. W., Kalk, K. H., Littlechild, J. A., Watson, H. C., & Hol, W. G. J. (1993) *Proc. Natl. Acad. Sci. U.S.A. 90*, 2355−2359.
Vellieux, F. M. D., Hajdu, J., & Hol, W. G. J. (1995) *Acta Crystallogr., Sect. D 51*, 575−589.
Verlinde, C. L. M. J., & Hol, W. G. J. (1994) *Structure 2*, 577−587.
Verlinde, C. L. M. J., Merritt, E. A., van den Akker, F., Kim, H., Feil, I., Delboni, L. F., Mande, S. C., Sarfaty, S., Petra, P. H., & Hol, W. G. J. (1994a) *Protein Sci. 3*, 1670−1686.
Verlinde, C. L. M. J., Callens, M., Van Calenbergh, S., Van Aerschot, A., Herdewijn, P., Hannaert, V., Michels, P. A. M., Opperdoes, F. R., & Hol, W. G. J. (1994b) *J. Med. Chem. 37*, 3605−3613.
Visser, N., Opperdoes, F. R., & Borst, P. (1981) *Eur. J. Biochem. 118*, 521−526.
Wang, C. C. (1995) *Annu. Rev. Pharmacol. Toxicol. 35*, 93−127.
Watson, H. C., Duee, E., & Mercer, W. D. (1972) *Nature New Biol. 240*, 130.

BI951665U